substance: titanium oxide (TiO_2)
property: properties of impurity-doped rutile

trivalent cations: Johnson Mathey Specpure TiO_2 powder contains cationic impurities; the number and concentration of impurities generally increases with sample treatment.

A typical starting powder contained Al^{3+} (32 ppm), Fe^{3+} (16 ppm), and Cr^{3+} (10 ppm) [77B2].

trivalent impurities;

(n, p: electron, hole concentration) defect configuration			
$2M_{Ti}' + V_0^{\cdot\cdot}$		analysis for M = Al at 1000...1500 K [63Y]; $M_{Ti}' = M^{3+}$ on Ti^{4+} lattice site	63Y
$(Ti - V_0)^{\cdot} = M_{Ti}' - V_0^{\cdot\cdot}$ pair	resonance peak in dielectric relaxation (T = 0...200°C)	activation energy for mobility of $V_0^{\cdot\cdot}$ about M_{Ti}': 0.13 eV	63Y, 58K
$(M_{Ti} - V_0) = M_{Ti}' - V_0^{\cdot}$ pair	resonance peak in dielectric relaxation (T < 20 K)	activation energy for mobility of $V_0^{\cdot}$ about M_{Ti}':$1 \cdot 10^{-3}$ eV	67D01
$3M_{Ti}' + M_i^{3\cdot}$	solubility Al_2O_3 in TiO_2 is 1...2 w%	$M_i^{3\cdot}$ = triply ionized impurity interstitial	69S
$M_i^{3\cdot}$	resonance peak in internal friction (T = 50°C)	activation energy for $M_i^{3\cdot}$ mobility: 0.66 eV	66W
$(M_i^{3\cdot} - Ti_i^{3\cdot})$	resonance peak in internal friction (200°C)	activation energy for $M_i^{3\cdot} - Ti_i^{3\cdot}$ rotation: 0.93eV	66W
$(M_{Ti} - Ti_i - M_{Ti})^{\cdot}$	resonance peak in dielectric relaxation (T = 16 K)	$Ti_i^{3\cdot}$ linearly coordinated by 2 M_{Ti}' activation energy $2 \cdot 10^{-2}$ eV	67D02
$(M_{Ti} - Ti_i)^{\cdot\cdot} = M_{Ti}' - Ti_i^{3\cdot}$ pair	ESR (S = 1/2)		72H

At high oxygen partial pressures, where oxygen vacancies are suppressed the principal defects at high temperatures appear to be quadruply ionized Ti-interstitials ($Ti_i^{4\cdot}$), substitutional M^{3+}-ions (M_{Ti}'), and Ti^{4+}-ion vacancies ($V_{Ti}^{4'}$) (see also below). Hence the general electroneutrality equation becomes $4[Ti_i^{4\cdot}] + p = n + [M_{Ti}'] + 4[V_{Ti}^{4'}]$, and the equilibrium constants are $K_1 = [Ti_i^{4\cdot}]\, n^4\, p_{O_2}$, $K_2 = [V_{Ti}^{4\cdot}]\, p^4\, p_{O_2}^{-1}$, $K_i = n{\cdot}p = K_i^0 \exp(-E_g/kT)$. With the assumption that $[V_{Ti}^{4'}] \approx 0$, the Seebeck data (Fig. 1) gives $E_g(T) = E_g(0) - \beta T$ where $E_g(0) = 3.2$ eV and $\beta = 6.6{\cdot}10^{-4}$ eV K^{-1} [77B2]. An independent value of β from photoconductivity measurements is $8.9{\cdot}10^{-4}$ eV K^{-1} [66B]. Analysis also gives K_1 as $2.4{\cdot}10^{84}$ at 1273 K, $5.3{\cdot}10^{89}$ at 1473 K and $7.5{\cdot}\ 10^{92}$ atm cm^{-15} at 1623 K. Similarly, $K_2K_i^{-4}$ takes the values $3.5{\cdot}10^{-58}$, $9.4{\cdot}10^{-61}$ and $4.1{\cdot}10^{-62}$ cm^9 atm^{-1} at the same temperatures [77B2]. Fig. 2 shows the conductivity of Al-doped TiO_2 as a function of oxygen partial pressure; the conductivity changes from n to p type with increasing p_{O_2} at the minimum conductivity. The critical p_{O_2} varies with T.

Nb-doped TiO_2: Rutile dissolves 4 to 8 at% Nb^{5+} at 1330 K under oxidizing conditions before $TiNb_2O_7$ appears [70E]. EPR evidence shows that the Nb^{5+} enters substitutionally [61C, 73Z] and for low doping $4[Ti_i^{4\cdot}] + p + [Nb_{Ti}^{\cdot}] = n + [Mn_{Ti}'] + 4[V_{Ti}^{4'}]$, since ionization is complete for $T > 30$ K [73Z]. At high p_{O_2} where point-defect model applies, Ti-vacancies may compensate Nb-interstitials, even reaching $4[V_{Ti}^{4'}] = [Nb_{Ti}^{\cdot}]$, to give $n = ([Nb_{Ti}^{\cdot}]/4K_2)^{1/4}\ K_i\ p_{O_2}^{-1/4}$ [77B2]. The resultant defect situation is shown schematically in Fig. 3 and the conductivity vs. p_{O_2} in Fig. 4, vs. Nb-content in Fig. 5. The Seebeck coefficients for three concentrations of Nb are shown in Fig. 6. For Seebeck coefficient and calculated effective masses, see Fig. 7. Similar behaviour is found for Ta-doped TiO_2 [80T].

Cr-doped TiO_2: For doping with M^{3+} ions such as Cr one has the equilibria $2M_2O_3 + Ti_{Ti} \leftrightarrow 4M_{Ti}' + Ti_i^{4\cdot} + 6O_O$

or under high oxygen pressure $M_2O_3 + 1/2\ O_2(g) \leftrightarrow 2M_{Ti}' + 4O_O + 2e^+$.

The local charge balance gives $4[Ti_i^{4\cdot}] + p = n + [M_{Ti}']$ and this gives rise to the defect situation of Fig. 8 [80T]. Conductivity vs. p_{O_2} at 1273 K (Fig. 9) shows an n-p transition. The crystal chemistry of the $Cr_2O_3 - TiO_2$ system is complex; shear phases are found close to pure TiO_2 and extensive CS phases in the intermediate region [70F, 72B, 74P, 78S, 79I]. At low Cr_2O_3 concentrations disordered CS planes lying on (253) planes of the rutile structure are found. As Cr_2O_3 increases, these CS planes become ordered in a series of oxides down to $(Ti,Cr)O_{1.93}$. Between $(Ti,Cr)O_{1.93}$ and $(Ti,Cr)O_{1.90}$ the planes swing round towards (121) and increasing the Cr_2O_3 content further gives a homologous series of oxides down to $(Ti,Cr)_6O_{11}$ at high temperatures and $Ti_6Cr_2O_{15}$ at low temperatures. The dc resistivity is given vs. T in Fig. 10 and the ac resistivity in Fig. 11.

other dopants: see [72M, 79M]. Some results are summarized in Fig. 12.

References:

58K Van Keymeulen, J.: Naturwissenschaften 45 (1958) 56.
61C Chester, P. F.: J. Appl. Phys. 32 (1961) 866.
63Y Yahia, J.: Phys. Rev. 130 (1963) 1711.
66B Bube, R. H.: Photoconductivity of Solids, New York: J. Wiley 1966, p. 237.
66W Wahlbeck, P. G., Gilles, P. W.: J. Am. Ceram. Soc. 49 (1966) 180.
67D1 Dominik, L. A. K., MacCrone, R. K.: Phys. Rev. 156 (1967) 910.
67D2 Dominik, L. A. K., MacCrone, R. K.: Phys. Rev. 163 (1967) 756.
69S Slepetys, R., Vaughan, P. A.: J. Phys. Chem. 73 (1969) 2157.
70E Eror, N. G., Smyth, D. M.: The Chemistry of Extended Defects in Non-Metallic Solids, L. Eyring and M. O'Keeffe, eds., N. Holland, 1970.
70F Flörke, O. W., Lee, C. W.: J. Solid State Chem. 1 (1970) 144.
72B Bursill, L. A., Hyde, H. G.: Prog. Solid State Chem. 7 (1972) 177.
72H Hasiguti, R.: Adv. Mater. Sci. 2 (1972) 69.
72K Kofstad, P.: Nonstoichiometry, Diffusion and Electrical Conductivity in Binary Metal Oxides, New York: Wiley, 1972.
72M Mizushima, K., Tanaka, M., Tida, S.: J. Phys. Soc. Jpn. 32 (1972) 1519.
73Z Zimmermann, P. H.: Phys. Rev. B8 (1973) 3917.
74P Philp, D. K., Bursill, L. A.: Acta Crystallogr. A30 (1974) 265.
77B1 Baumard, J. F., Tani, E.: J. Chem. Phys. 67 (1977) 3018.
77B2 Baumard, J. F., Tani, E.: Phys. Status Solidi (a) 39 (1977) 373.
78C Cristea, V., Babes, V.: Phys. Status Solidi (a) 48 (1978) 617.
78S Somiya, S., Hirano, S., Kamiya, S.: J. Solid State Chem. 25 (1978) 273.
79I Inoue, A., Iguchi, E.: J. Phys. C12 (1979) 5157.
79M Mizushima, K., Tanaka, M., Asai, A., Iida, S., Goodenough, J. B.: J. Phys. Chem. Solids 40 (1979) 1129.
80T Tani, E., Baumard, J. F.: J. Solid State Chem. 32 (1980) 105.

Fig. 1.

TiO_2:Nb. Seebeck coefficient at p_{O2} = 10^{-10} atm and K_i (= $K_i^0 \exp(-E_g/kT)$ vs. reciprocal temperature for Nb-doped polycrystalline TiO_2 [77B2].

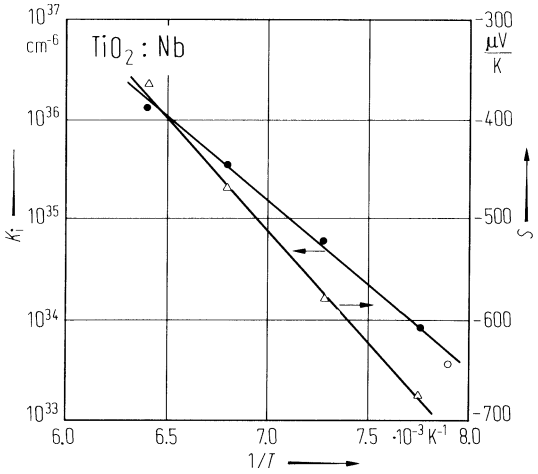

Fig. 2.

TiO_2:Al. Carrier and vacancy concentrations at 900ºC vs. oxygen pressure for 0.5 at% Al-doped material and comparison with the conductivity [72K, 63Y].

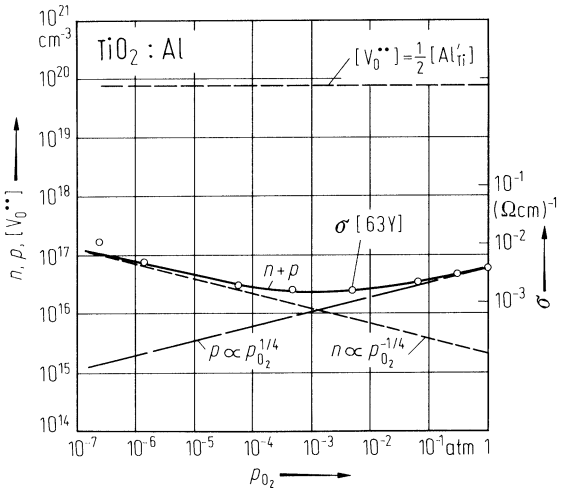

Fig. 3.

TiO_2:Nb. Defect equilibria. The parameter α is the charge on Ti-vacancies and is assumed equal to 4. It is also assumed that $[Nb_{Ti}^{\cdot}] >> K_i^{1/2} >> (K_1K_2)^{1/2}K_i^{-2}$ [77B1]. Region A: low p_{O_2}, concentration of native defects prevails over doping effect; B: electron concentration n is not dependent on p_{O_2}, C: high p_{O_2}, an overstoichiometric $Nb_yTi_{1-y}O_{2+y/2}$ is expected owing to the rapid variation of $[Ti_i^{4\cdot}]$ and $[V_{Ti}^{\alpha'}]$ in B. See also Fig. 8.

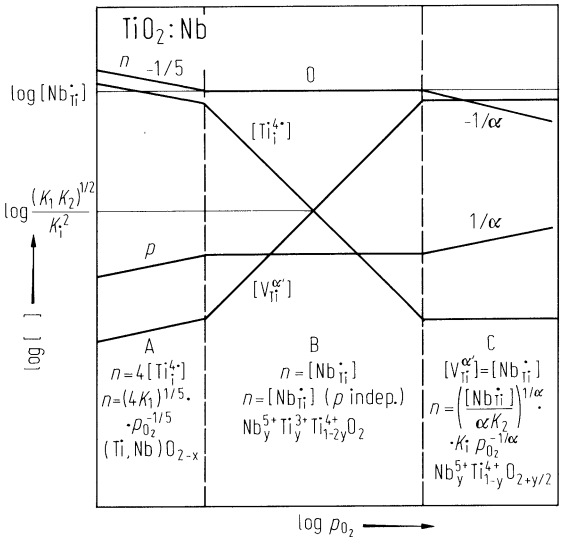

Fig. 4.

TiO_2:Nb. Conductivity vs. oxygen partial pressure for polycrystalline Nb-doped material. (a) 1473 K, (b) 1623K. *1*: pure TiO_2, Nb/Ti ratio: 0.0004 (*2*), 0.001 (*3*), 0.003 (*4*), 0.01 (*5*), 0.03 (*6*). Full lines: calculated curves using a point defect model. For (*2*), dashed curve is calculated with 100 ppm counterdopant. Dotted line: influence of intrinsic effects [77B1].

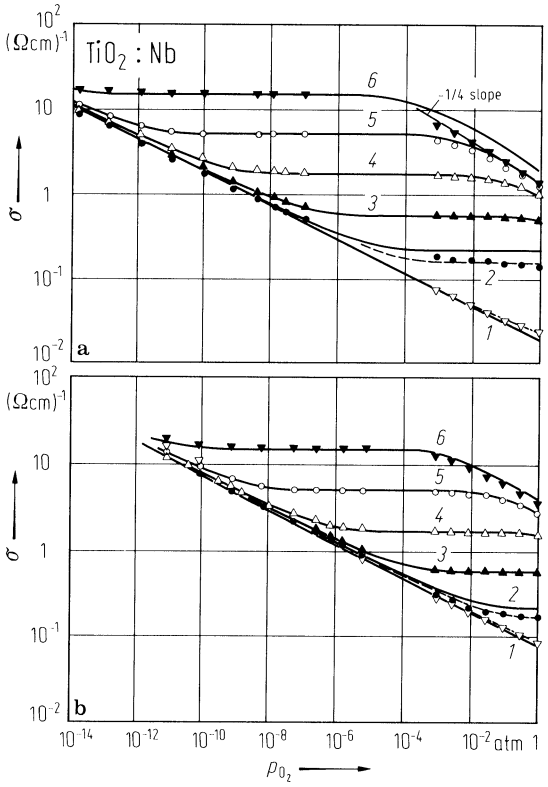

Fig. 5.

TiO_2:Nb. Conductivity vs. Nb-concentration at 1273 K, $p_{O_2} = 10^{-10}$ atm [77B1]. Polycrystalline sample.

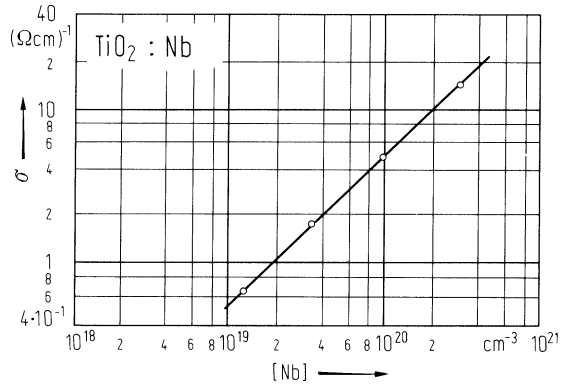

Fig. 6.

TiO_2:Nb. Seebeck coefficient vs. oxygen partial pressure for three polycrystalline samples. T = 1473 K (open circles), 1273 K (full circles); (a) 1 at% Nb, (b) 0.1 at% Nb, (c) 0.01 at% Nb. In (c) the influence of trivalent impurities is clearly seen. Calculated curves: — zero, --- 75 ppm, -.-.- 125 ppm trivalent impurities [77B2].

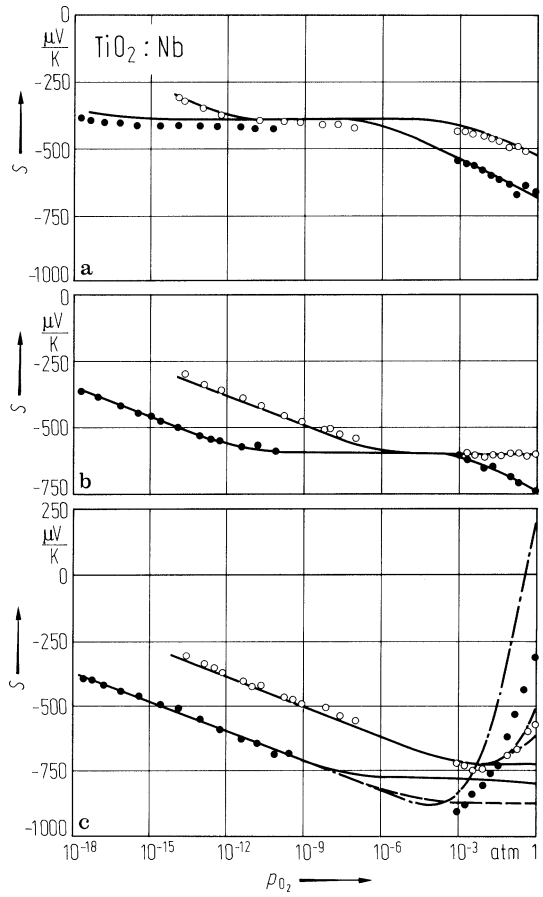

Fig. 7.

TiO_2:Nb. a) Seebeck coefficient vs. temperature for eight Nb-doped single crystal TiO_2 samples measured along the *c*-axis. b) Effective masses vs. temperature for the same samples [78C].

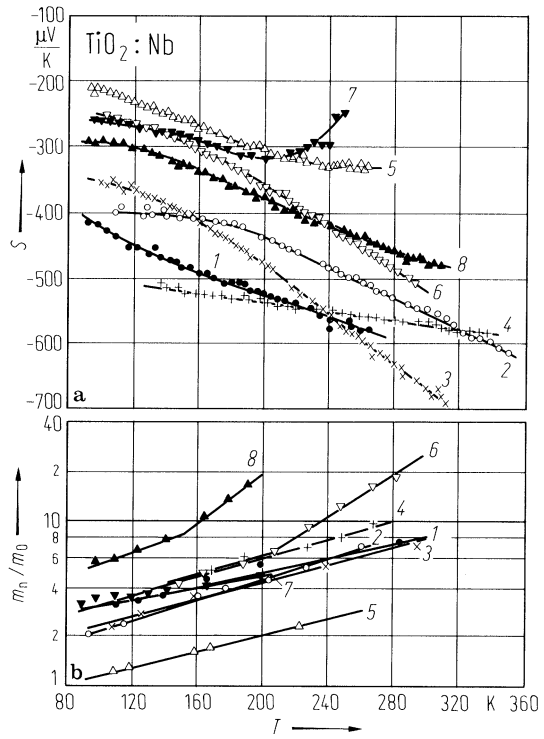

Fig. 8.

TiO_2:M. Variation of the defect concentrations *n*, *p*, $[Ti_i^{4\cdot}]$ and $[V_{Ti}^{4'}]$ vs. oxygen partial pressure for TiO_2 doped with M^{3+}. The regions A...C correspond to ranges of different behaviour as indicated [80T].

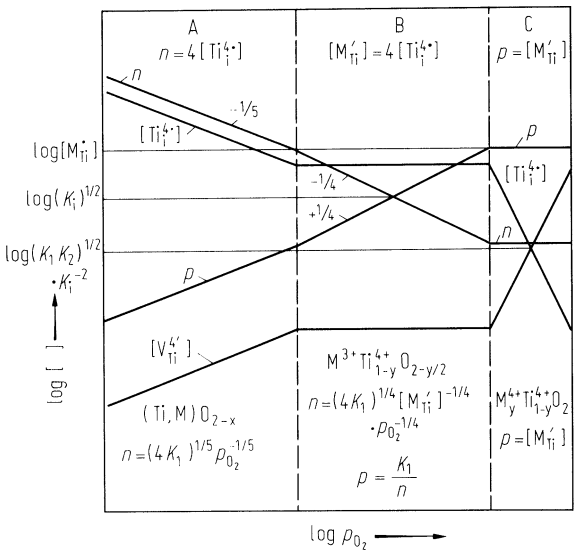

Fig. 9.

TiO_2:Cr. Conductivity of polycrystalline Cr:TiO_2 of various atomic ratios vs. oxygen partial pressure at (a) 1273 K (b) 1473 K. Full lines are best fit from defect model described in the text [80T].

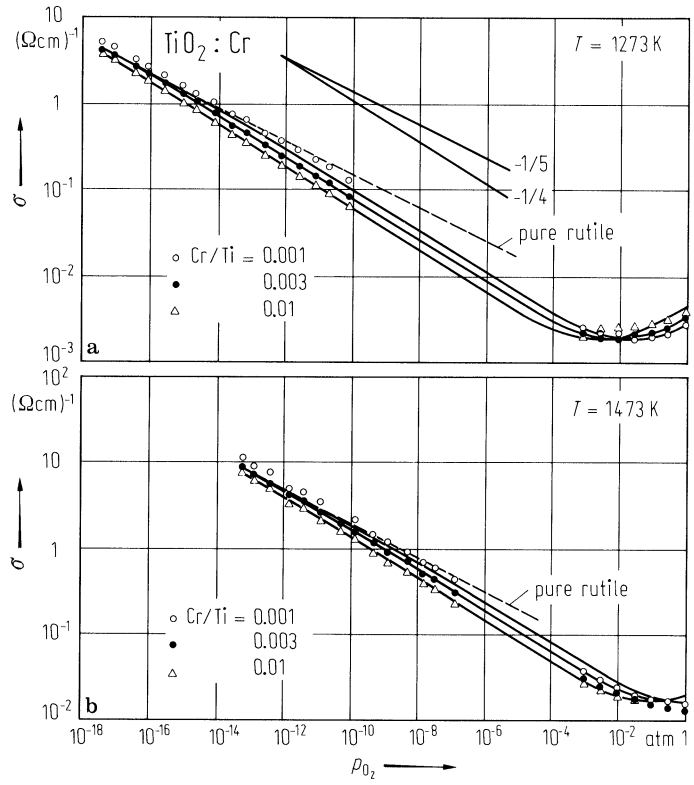

Fig. 10.

TiO_2:Cr. dc electrical resistivity of single crystal slices in the *c*-direction vs. reciprocal temperature. The slices were doped by heating with powdered Cr_2O_3. The heating times were between 4 weeks (upper curve) and 3 h (lowest curve) [79I].

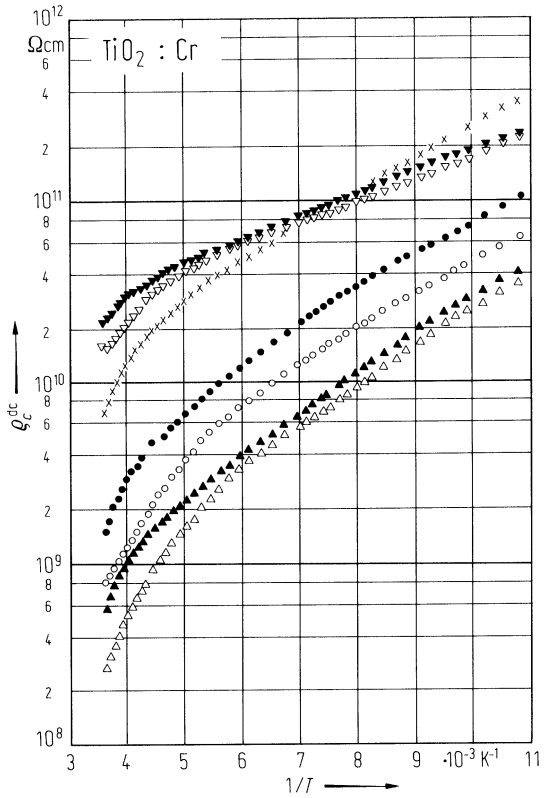

Fig. 11.

TiO_2:Cr. ac electrical resistivity vs. frequency at 293 K in the *c*-direction. Samples prepared as in Fig. 10; heating times: A 1 day, B 2 days, C 2 weeks [79I].

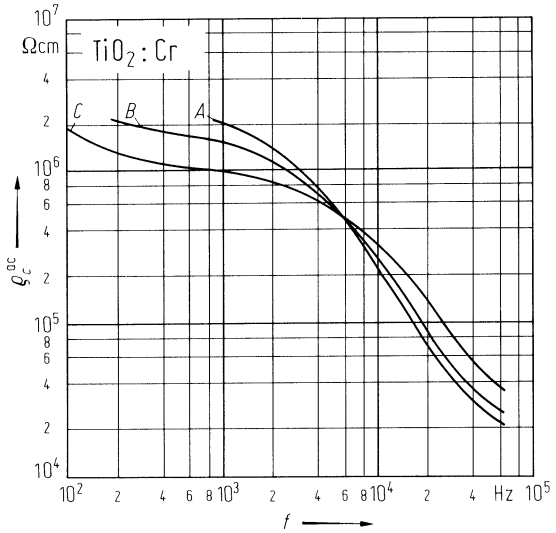

Fig. 12.

TiO_2. Binding energies of transition-metal impurities in TiO_2 from epr and photoconductivity measurements [79M].